Available online at www.sciencedirect.com
ScienceDirect
Nuclear Instruments and Methods in Physics Research B 258 (2007) 21–27
NIM B
Beam Interactions with Materials & Atoms
www.elsevier.com/locate/nimb

Axial grazing collisions with insulator surfaces

M.S. Gravielle *, J.E. Miraglia

Instituto de Astronomía y Física del Espacio (IAFE), Consejo Nacional de Investigaciones Científicas y Técnicas, Casilla de Correo 67, Sucursal 28, 1428 Buenos Aires, Argentina
Departamento de Física, FCEN, Universidad de Buenos Aires, Argentina

Available online 22 December 2006

Abstract

Electron capture and emission processes from insulator surfaces produced by grazing impact of fast ions are investigated under axial incidence conditions. For crystal surfaces we develop a model based on distorted wave methods, which allows us to express the coherent transition amplitude along the projectile path as a sum of atomic amplitudes, each one associated with a different lattice site. The method is applied to 100 keV protons colliding with LiF surfaces. For electron transitions from a given initial crystal state, the probabilities display strong interference effects as a function of the crystal orientation. But the interference patterns disappear when these partial probabilities are added to derive the total probability from the surface band.

PACS: 34.50.Dy; 34.50.Bw

Keywords: Ion; Surface; Collision; Channeling; Interference

1. Introduction

For grazing impact of heavy ions on crystal surfaces, two different collision models – planar and axial – can be considered [1]. The planar model applies to a random orientation of the projectile trajectory with respect to the crystal axes, while the axial one is related to ions moving along precise strings of surface atoms. We are interested in this last process, which is expected to reveal signatures of the periodic structure of the solid [2–6].

Under axial scattering conditions, electronic transitions from insulator surfaces can be seen as a collection of individual processes from the different ionic centers of the crystal lattice. The corresponding transition amplitudes must be coherently added in order to derive the transition probability along the projectile path, which gives rise to interference effects [7]. The present work focuses on the coherence phenomena associated with the electron capture and emission from insulator surfaces at intermediate and high impact velocities. To describe both processes we extend the use of distorted-wave methods to deal with a crystal surface, formed by a large collection of atoms, as a target. For electron capture we employ the eikonal impulse (EI) approach [8], while for electron emission we use the continuum-distorted-wave-eikonal-initial-state (CDW-EIS) approximation [9]. Both theories include the proper projectile and target distortions in the initial and final channels, respectively, and have proved an effective tool to explain experimental data for a large variety of ion–atom collisions [8,10,11].

The proposed method is here applied to study the electron exchange and emission processes induced by grazing scattering of fast protons from LiF(100) surfaces. For axial incidence we found that the electron transition probabilities from a given initial state display oscillatory patterns as a function of the orientation of the projectile trajectory. Notably, these interference structures almost completely disappear when the partial contributions

* Corresponding author. Tel.: +54 11 47 81 67 55; fax: +54 11 47 86 81 14.
E-mail address: msilvia@iafe.uba.ar (M.S. Gravielle).

0168-583X/$ - see front matter © 2006 Elsevier B.V. All rights reserved.
doi:10.1016/j.nimb.2006.12.083

coming from different initial crystal states are added to derive the total probability from the surface band.

Throughout this article, atomic units are used unless otherwise stated.

2. Theoretical model

Let us consider a heavy projectile (P), with charge z_P, grazingly impinging on a orthorhombic crystal surface (S). As a result of the collision, an electron (e), initially bound to the crystal in the surface band i, ends in the final state f. Within the impact parameter formalism, the motion of the incident ion is classically represented, while the electronic transition is described with quantum methods. We consider that the whole trajectory of the projectile is contained in a unique plane (scattering plane), which forms a angle α with respect to the crystal axes. The frame of reference is placed on a target nucleus belonging to the first atomic layer, with the $\hat{x}$ and $\hat{y}$ versors coinciding with the lattice axis.

For insulators, as the electrons are strongly localized around the ionic centers of the crystal lattice, the projectile affects mainly electrons belonging to the first atomic layer. Then, the initial unperturbed state ϕ_i, associated with the electron bound to the crystal surface, can be represented by using the tight-binding method [12] as

$$\phi_i \equiv \phi_{i\vec{k}}(\vec{r}) = \sum\nolimits_{n,m=-\infty}^{+\infty} e^{i\vec{k}\cdot\vec{x}_{nm}} \varphi_i(\vec{r}-\vec{x}_{nm}), \tag{1}$$

where $\vec{r}$ is the position vector of the active electron e and the wave vector $\vec{k} = k_x\hat{x} + k_y\hat{y} \equiv (k_x, k_y)$ has been introduced to identify a given crystal state within the surface band i, with $\vec{k}$ belonging to the first Brillouin zone. In Eq. (1), the function φ_i represents a Wannier function and the position vectors

$$\vec{x}_{nm} = nd_x\hat{x} + md_y\hat{y} \tag{2}$$

with $n, m = 0, \pm 1, \pm 2, \ldots$, determine lattice sites corresponding to surface atoms, d_x and d_y being the shortest inter-atomic distances in the directions $\hat{x}$ and $\hat{y}$, respectively.

Taking into account that for insulator materials the overlap between wave functions corresponding to nearest–neighbour ionic centers is small, we can approximate the Wannier function φ_i to the atomic wave function, corresponding to the isolated target ion. The energy ϵ_i of initial unperturbed state $\phi_{i\vec{k}}$ can be roughly expressed as [12]

$$\epsilon_i \equiv \epsilon_i(\vec{k}) = \varepsilon_i - \frac{\delta_i}{2}\cos(k_x d_x)\cos(k_y d_y), \tag{3}$$

where ε_i is the eigenenergy associated with the atomic state φ_i and δ_i is the bandwidth.

2.1. Coherent transition amplitude

In this work the electron capture and emission from crystal surfaces are described by employing the EI and CDW-EIS approximations, respectively. Both distorted wave methods make use of the eikonal wave function to represent the distorted electronic state in the initial channel. The corresponding transition amplitudes read

$$A_{i\vec{k}}^{(s)} = -i\int_{-\infty}^{+\infty} dt \left\langle \chi_f^{(s)-} \middle| V_f^{(s)\dagger} \middle| \chi_{i\vec{k}}^{+} \right\rangle, \quad s = c, e, \tag{4}$$

where the index s denotes electron capture (c) or electron emission (e) transitions. The function $\chi_{i\vec{k}}^{+}(\chi_f^{(s)-})$ represents the initial (final) distorted wave function, with outgoing (incoming) asymptotic conditions, and $V_f^{(s)}$ is the perturbative potential in the final channel, with s = c, e. For surface targets the initial eikonal wave function reads

$$\chi_{i\vec{k}}^{+} = \phi_{i\vec{k}}(\vec{r}) E^{+}(z_P, -\vec{v}, \vec{r}_P) \exp[-i\epsilon_i(\vec{k})t], \tag{5}$$

where $E^{+}(z_P, -\vec{v}, \vec{r}_P) = \exp[-iz_P/v \ln(v r_P + \vec{v}\cdot\vec{r}_P)]$ is the eikonal phase that describes the asymptotic distortion produced by the projectile in the entrance channel, with $\vec{v}$ the component of the projectile velocity parallel to the surface, $\vec{r}_P$ the position vector of e with respect to P and $r_P = |\vec{r}_P|$.

For the charge exchange process, within the EI approach the exact impulse wave function $\chi_f^{(c)-}$ is used in the final channel. It reads

$$\chi_f^{(c)-} = \frac{1}{(2\pi)^{3/2}} \int d\vec{q}\, \tilde{\varphi}_f^{(c)}(\vec{q}) \exp(i\vec{q}\cdot\vec{r}_P) \mathscr{D}_S^{-}(\vec{q}+\vec{v}, \vec{r}) \times \exp(-i\varepsilon_f^{(c)}t) \exp(i\vec{v}\cdot\vec{r} - iv^2 t/2), \tag{6}$$

where $\varphi_f^{(c)}$ is the final state associated with the electron bound to the projectile with eigenenergy $\varepsilon_f^{(c)}$ and the tilde denotes the Fourier transform. The function $\mathscr{D}_S^{-}(\vec{p}, \vec{r})$ represents the distortion introduced by the crystal surface in the exit channel and the last exponential factor (translation factor) takes into account that the projectile is moving in the frame of reference.

For electron emission, instead, we employ the final continuum-distorted-wave function $\chi_f^{(e)-}$ within the CDW-EIS approximation. The function $\chi_f^{(e)-}$ reads

$$\chi_f^{(e)-} = \varphi_f^{(e)}(\vec{r}) \mathscr{D}_S^{-}(\vec{k}_e, \vec{r}) D^{-}(z_P, \vec{k}_P, \vec{r}_P) \exp(-i\varepsilon_f^{(e)}t), \tag{7}$$

where $\varphi_f^{(e)}(\vec{r}) = (2\pi)^{-3/2} \exp(i\vec{k}_e\cdot\vec{r})$ is the final unperturbed state corresponding to the electron ejected with momentum $\vec{k}_e$, and $\varepsilon_f^{(e)} = k_e^2/2$ is its eigenenergy. In Eq. (7), $\vec{k}_P = \vec{k}_e - \vec{v}$ is the electron momentum with respect to P, and $D^{-}(z_P, \vec{p}, \vec{r}) = \exp(\pi z_P/(2p)) \Gamma(1 + iz_P/p)\, {}_1F_1(-iz_P/p, 1, -ipr - i\vec{p}\cdot\vec{r})$ represents the Coulomb distortion factor that takes into account the action of the projectile on the emitted electron, with ${}_1F_1$ the confluent hypergeometric function and $p = |\vec{p}|$.

By replacing the corresponding distorted wave functions in Eq. (4) the coherent transition amplitude is expressed as

$$A_{i\vec{k}}^{(s)} = \sum_{n,m=-\infty}^{+\infty} \exp[i(\vec{k} - \vec{W}_s)\cdot\vec{x}_{nm}] \mathscr{A}_i^{(s)}(\vec{x}_{nm}) \tag{8}$$

for s = c, e, where the function $\mathscr{A}_i^{(s)}(\vec{x}_{nm})$ is related to the electronic transition from the atomic bound state $\varphi_i(\vec{r} - \vec{x}_{nm})$, which is centered around the position $\vec{x}_{nm}$ of the lattice. The vectors $\vec{W}_s$, for s = c, e, are associated with

the momentum transfer during the transition. For electron capture, the transferred momentum vector reads

$$\vec{W}_{\rm c} = \left(\frac{v}{2} + \frac{\epsilon_{\rm i}(\vec{k}) - \varepsilon_{\rm f}^{(\rm c)}}{v}\right)\hat{v} \tag{9}$$

with $\hat{v} = \vec{v}/v$, while for electron emission,

$$\vec{W}_{\rm e} = \vec{k}_{\rm e} + \left(\frac{\epsilon_{\rm i}(\vec{k}) - \varepsilon_{\rm f}^{(\rm e)}}{v}\right)\hat{v}. \tag{10}$$

We assume that when the electron e comes from a region close to the $\vec{x}_{nm}$ site, only the time interval in which the projectile moves close to the position $\vec{x}_{nm}$ contributes effectively to the transition. In addition, as passive electrons fully screen the other ionic centers in the exit channel, the final interaction between e and the ionic core placed at the position $\vec{x}_{nm}$ can be represented by a Coulomb potential with an effective charge $z_{\rm T} = \sqrt{-2n_{\rm i}^2\varepsilon_{\rm i}}$, where $n_{\rm i}$ is the principal quantum number associated with $\varphi_{\rm i}$. Consequently, the function $\mathscr{A}_{\rm i}^{(\rm s)}(\vec{x}_{nm})$ becomes equal to the amplitude for the atomic transition $\varphi_{\rm i} \to \varphi_{\rm f}^{(\rm s)}$; i.e. $\mathscr{A}_{\rm i}^{(\rm s)}(\vec{x}_{nm}) = a_{\rm i}^{\rm at(s)}(\vec{\rho}_{nm})$, where $\vec{\rho}_{nm}$ is the impact parameter measured with respect to site $\vec{x}_{nm}$, with $\vec{\rho}_{nm}\cdot\vec{v} = 0$ and s = c, e (see [7] for details).

In this way, the coherent amplitude associated with the electron transition from the crystal surface can be expressed as

$$A_{\vec{\rm i}\vec{k}}^{(\rm s)} = \sum_{n,m=-\infty}^{+\infty} \exp[{\rm i}(\vec{k} - \vec{W}_{\rm s})\cdot\vec{x}_{nm}]a_{\rm i}^{\rm at(s)}(\vec{\rho}_{nm}) \tag{11}$$

for s = c, e. From Eq. (11) the process looks like a collection of individual atomic transitions, each of them from a different site $\vec{x}_{nm}$ of the lattice.

2.2. Coherent transition probability

For a fixed incidence direction, the different projectile paths can be identified by means of the vector $\vec{R}_0 = (X_0, Y_0, 0)$ that determines the position on the surface plane where projectile reaches the closet distance to the surface. By averaging $\vec{R}_0$ in a unit surface cell, the electron transition probability from a given crystal state $\phi_{\vec{\rm i}\vec{k}}$ within the surface band i is expressed as

$$P_{\vec{\rm i}\vec{k}}^{(\rm s)} = \frac{u_{\rm s}}{S_0}\int_{S_0} {\rm d}\vec{R}_0 \left|A_{\vec{\rm i}\vec{k}}^{(\rm s)}\right|^2, \quad {\rm s} = {\rm c}, {\rm e}, \tag{12}$$

where $A_{\vec{\rm i}\vec{k}}^{(\rm s)}$ is the coherent transition amplitude, given by Eq. (11), $S_0 = 2d_x d_y$ is the integration area, and $u_{\rm s} = 1$ ($k_{\rm e}$) for s = c (e). The probability $P_{\vec{\rm i}\vec{k}}^{(\rm s)}$, with s = c, e, will be here named partial-band probability for electron capture and emission, respectively. Note that in the case of electron emission, $P_{\vec{\rm i}\vec{k}}^{(\rm e)}$ represents the differential partial-band probability $P_{\vec{\rm i}\vec{k}}^{(\rm e)} \equiv {\rm d}\mathscr{P}_{\vec{\rm i}\vec{k}}^{(\rm e)}/{\rm d}\varepsilon_{\rm f}^{(\rm e)}{\rm d}\Omega_{\rm f}$ corresponding to the ejection of electrons with momentum $\vec{k}_{\rm e}$ in the direction $\Omega_{\rm f}$.

The total-band probability that takes into account contributions coming from the different initial crystal states within the surface band is obtained from Eq. (12) as

$$P_{\rm i}^{(\rm s)} = \frac{1}{\mathscr{S}_{\rm B}}\int_{\mathscr{S}_{\rm B}} {\rm d}\vec{k} P_{\vec{\rm i}\vec{k}}^{(\rm s)}, \quad {\rm s} = {\rm c}, {\rm e}, \tag{13}$$

where $\mathscr{S}_{\rm B} = (2\pi)^2/S'$ is the area of the first Brillouin zone, with S' the surface of the primitive cell of the direct lattice [12].

3. Results

Our study of the coherent electron transitions from insulator surfaces is confined to 100 keV protons colliding with a LiF(1 0 0) surface with a glancing incidence angle ($\theta_{\rm i} = 0.7°$). Since LiF is a typical example of insulator material, this collisional system has received large attention, theoretically and experimentally, in the last past years [13–16].

At the considered impact energy, the projectile mostly induces electron transitions from the K-shell of Li^+ cations and the L-shell of F^- anions, which are placed at alternate sites of a cubic lattice. For electron capture we consider the electron transfer to the ground state of hydrogen, which provides the most important contribution to the proton neutralization. For electron emission, we analyze the ejection of electrons in the scattering plane with a fixed angle $\theta_{\rm e}$, measured with respect to the surface plane. In particular, we choose the angle $\theta_{\rm e} = 20°$, for which the electron spectrum associated with the atomic collision does not display any particular structure. That is, in this angular region convoy and binary peaks are absent from the electron energy distributions [16], allowing us to appreciate contributions coming from coherence phenomena without superimposed structures.

The atomic transition amplitudes corresponding to the electron capture and emission processes were evaluated by using the standard EI [8] and CDW-EIS [11] approximations, respectively. The classical trajectory of the projectile was determined employing the Ziegler–Biersack–Littmark (ZBL) potential [17] to describe the projectile-surface interaction. Particulars about numerical calculations are given in [7].

3.1. Partial-band probabilities

We begin the analysis by considering a particular crystal state within the surface bands $Li^+(1s)$, $F^-(2s)$, $F^-(2p_0)$, and $F^-(2p_1)$. Partial-band probabilities from initial crystal states with $\vec{k} = (0, 0)$ are displayed in Figs. 1 and 2 for electron capture and emission, respectively. They are plotted as a function of the angle α that determines the orientation of the scattering plane with respect to the crystal axes. Due to the symmetry of the problem, only α-values ranging from 0 to $\pi/4$ are shown. In both figures the probabilities display strong interference effects as a function of the orientation of the crystal. We found that the

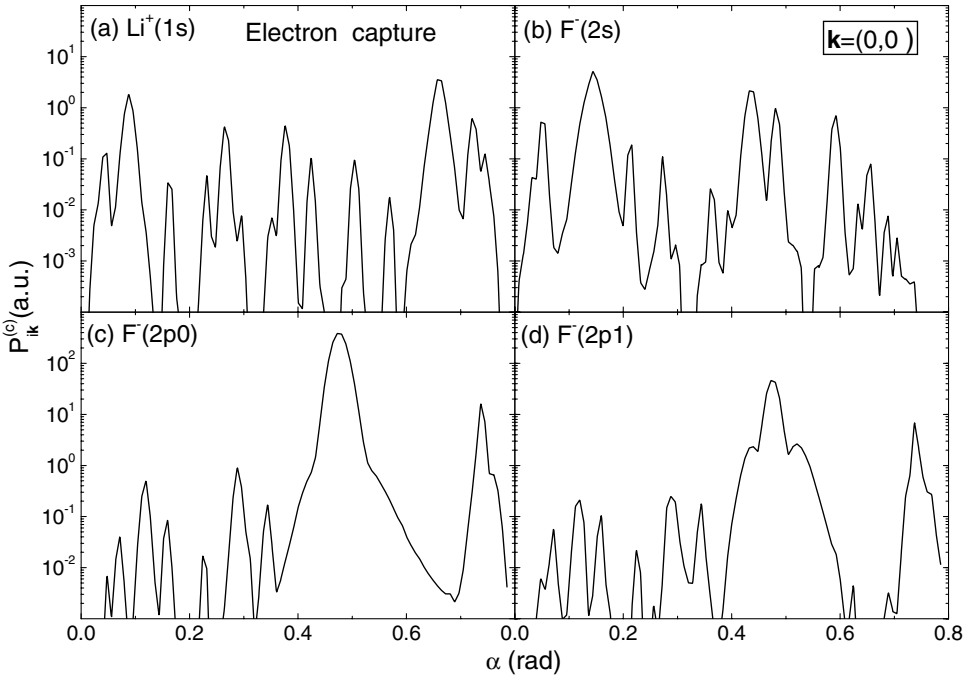

Fig. 1. Partial-band probabilities $P_{i\vec{k}}^{(c)}$, as given by Eq. (12), for electron capture from initial crystal states with $\vec{k} = (0, 0)$, as a function of the angle α that determines the orientation of the trajectory. The following initial surface bands are considered: (a) $Li^+(1s)$, (b) $F^-(2s)$, (c) $F^-(2p_0)$, and (d) $F^-(2p_1)$.

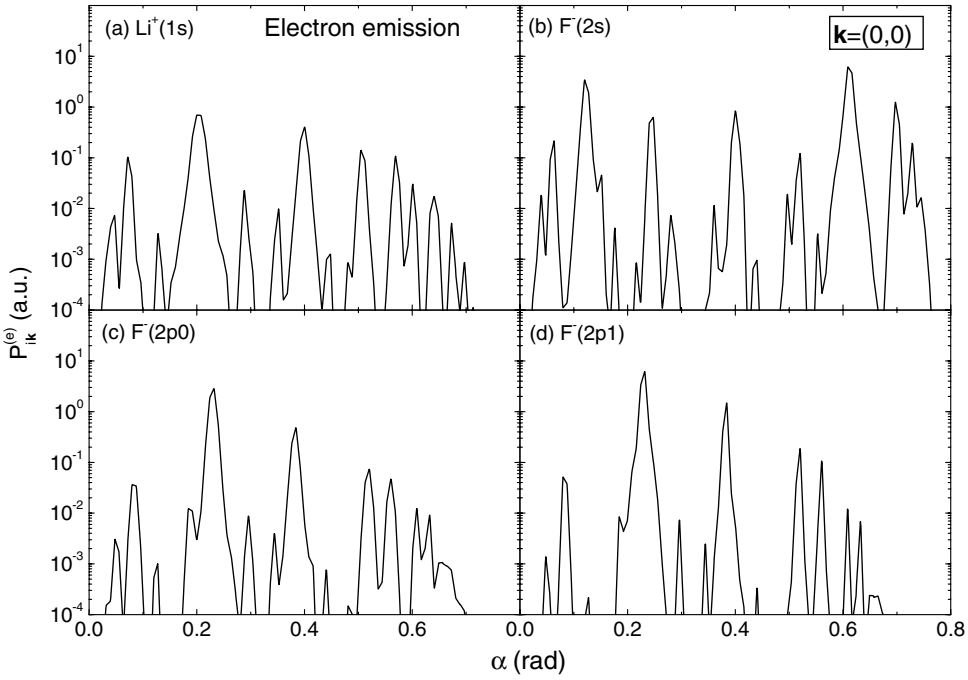

Fig. 2. Similar to Fig. 1 for electron emission in the scattering plane, with the electron ejection angle $\theta_e = 20°$ and the final electron energy $\varepsilon_f^{(e)} = 3.4$ a.u.

transition probability from a given initial state peaks up when the projectile moves along preferential directions of the crystal surface, while for other orientations of the trajectory the process is almost suppressed. Note that the directions along which partial-band probabilities display maxima do not necessarily coincide with low-index crystallographic directions, and they depend on the considered surface band, wave vector $\vec{k}$ and electronic process.

The origin of these interference effects can be roughly understood as follows: Since atomic transition amplitudes vary smoothly with the impact parameter, in a first

Figure 3

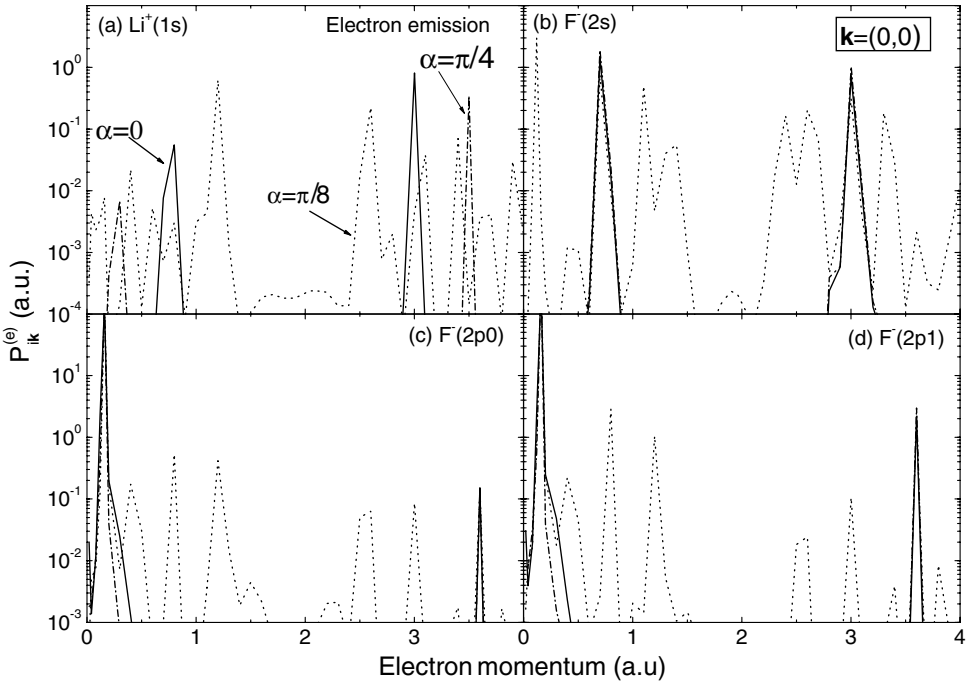

Fig. 3. Partial-band probabilities $P^{(e)}_{i\vec{k}}$, as a function of the electron momentum, for electron emission from initial crystal states with $\vec{k} = (0, 0)$. The ejection angle of the electron is $\theta_e = 20°$. Three different orientations of the projectile trajectory are considered: solid line, $\alpha = 0$; dotted line, $\alpha = \pi/8$; dot-dashed line, $\alpha = \pi/4$.

approach it is possible to extract them from the sum in Eq. (11). Then, maxima and minima of $P^{(s)}_{i\vec{k}}$ are essentially governed by the exponential weight factor that depends on $\vec{k} - \vec{W}_s$, with $s = c, e$. Partial-band probabilities $P^{(s)}_{i\vec{k}}$ will present a maximum for scattering along surface-ion strings that verify $(\vec{k} - \vec{W}_s) \cdot \hat{v} \simeq N2\pi/d$, with d the spacing between adjacent ions of the string, N small integer numbers, and $s = c, e$.

The oscillatory patterns observed in the partial-band probabilities could be experimentally detected by measuring the electronic transitions from the surface in coincidence with the filling of the $\vec{k}$-vacancy, which would allow to determine the initial electronic state. Note that for electron transfer, coherent capture amplitudes must be convoluted with the ones corresponding to coherent electron loss in order to compare with the experimental data of the charge state of the projectile. For electron emission, instead, coherent electron spectra could be directly contrasted with experiments, becoming a tool to study properties of the crystal states.

Partial-band probabilities for emission from initial crystal states with $\vec{k} = (0, 0)$ are plotted in Fig. 3 as a function of the final electron momentum, considering projectile trajectories along three different crystallographic directions. We observe that the electron emission spectra markedly depend on the crystal orientation. They display prominent structures, whose positions and shapes vary not only with the incidence direction of the projectile but also with the considered initial band.

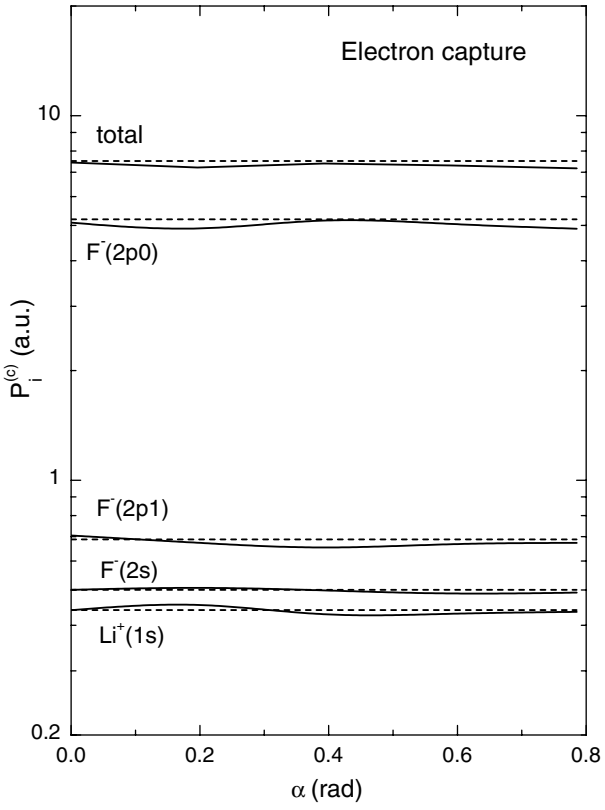

Fig. 4. Total-band probability for electron transfer from the surface bands $Li^+(1s)$, $F^-(2s)$, $F^-(2p_0)$, and $F^-(2p_1)$, as a function of the angle α. Solid line, coherent probability $P^{(c)}_i$, as given by Eq. (13); dashed line, incoherent capture probability.

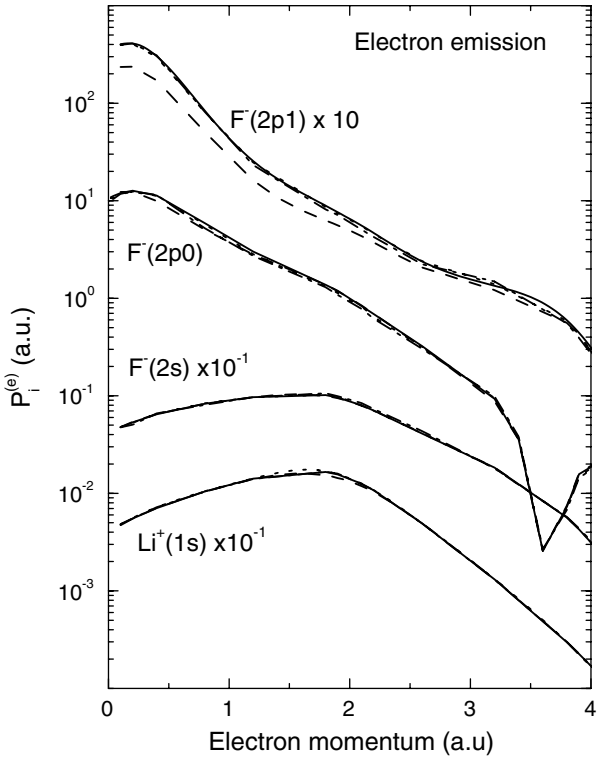

Fig. 5. Total-band probability for electron emission with the angle $\theta_e = 20°$, as a function of the electron momentum, for the surface bands $Li^+(1s)$, $F^-(2s)$, $F^-(2p_0)$, and $F^-(2p_1)$. Solid, dotted and dot-dashed lines, coherent probability $P_i^{(e)}$, as given by Eq. (13), for the orientation angles $\alpha = 0$, $\alpha = \pi/8$ and $\alpha = \pi/4$, respectively; dashed line, incoherent emission probability.

3.2. Total-band probabilities

Total-band probabilities for electron capture and emission are plotted in Figs. 4 and 5, respectively, as a function of the angle α that determines the crystal orientation. These probabilities were obtained by adding contributions coming from different crystal states $\phi_{i\vec{k}}$, as indicated in Eq. (13). Remarkably, the interference patterns produced by the coherent electronic transitions from different lattice sites disappear when the total-band probability is considered. Total results derived from Eq. (13) coincide quite well with the incoherent probabilities, corresponding to a random incidence. The incoherent probability is usually obtained by integrating the square modulus of the atomic transition amplitude on the surface plane, under the assumption that the surface ions form an uniform plane [16,18].

The explanation of such disappearance of the interference effects is based on the fact that for high impact velocities, the transferred momentum varies slightly with $\vec{k}$ and can be considered as a constant. Therefore, the integration on $\vec{k}$ involved in Eq. (13) can be analytically solved, leading to the incoherent limit of the probability, as explained in [7].

At this point, we must mention that the use of a more detailed description for the projectile trajectory could affect the present results, increasing the coherent probability especially for $\alpha \approx 0$ and $\alpha \approx \pi/4$, where the incident ion moves under low-index crystallographic channeling conditions [19].

4. Conclusions

We have presented a model to describe the coherent electronic transitions from insulator surfaces produced by grazing impact of fast ions. In particular, we have concentrated on the electron capture and emission processes from mono-crystal surfaces under axial scattering conditions. In this model, the transition amplitude is expressed as a coherent sum of atomic transition amplitudes, each of them associated with only one lattice site.

We found that the partial-band probabilities corresponding to electronic transitions from a given initial crystal state exhibit strong signatures of coherence phenomena associated with the periodicity of crystal lattice. These partial probabilities display sharp maxima for scattering along preferential directions of the crystal, which do not necessarily coincide with low-index crystallographic directions.

Notably, the interference structures disappear when the contributions from different crystal states are added to obtain the total-band probability from the surface band. For both processes – electron exchange and emission – the total probability for the coherent transition tends to the value corresponding to random incidence, usually known as incoherent probability. Although a more detailed description of the initial electronic states could modify our findings, we expect that accurate measurements of electron spectra, in coincidence with secondary processes related to the filling of the hole in the surface band, will allow to observe the footprints of the coherence effects. At present we are investigating the influence of the axial projectile trajectories, derived from a punctual description of the surface interaction [20], on the coherent transitions.

Acknowledgements

Financial support from the ANPCyT, CONICET, and UBACyT are acknowledged and greatly valued.

References

[1] H. Winter, Phys. Rep. 367 (2002) 387.
[2] F.J. García de Abajo, V.H. Ponce, P.M. Echenique, Phys. Rev. Lett. 69 (1992) 2364.
[3] F.J. García de Abajo, Nucl. Instr. and Meth. B 125 (1997) 1.
[4] K. Kimura, H. Ida, M. Fritz, M. Mannami, Phys. Rev. Lett. 76 (1996) 3850.
[5] C. Auth, A. Mertens, H. Winter, A.G. Borisov, F.J. García de Abajo, Phys. Rev. Lett. 79 (1997) 4477.
[6] Y. Nakai et al., Nucl. Instr. and Meth. B 230 (2005) 90.
[7] M.S. Gravielle, J.E. Miraglia, Phys. Rev. A 71 (2005) 032901.
[8] M.S. Gravielle, J.E. Miraglia, Phys. Rev. A 44 (1991) 7299.
[9] D.S.F. Crothers, J.F. McCann, J. Phys. B 16 (1983) 3229.
[10] M.S. Gravielle, J.E. Miraglia, Phys. Rev. A 51 (1995) 2131.

[11] P.D. Fainstein, V.H. Ponce, R.D. Rivarola, J. Phys. B 24 (1991) 3091.
[12] N.W. Ashcroft, N.D. Mermin, Solid State Physics, Holt, Rinehart and Winston, USA, 1976.
[13] K. Kimura, G. Andou, K. Nakajima, Nucl. Instr. and Meth. B 164–165 (2000) 933.
[14] G.R. Gómez, O. Grizzi, E.A. Sánchez, V.H. Ponce, Phys. Rev. B 58 (1998) 7403.
[15] V.H. Ponce, L.F. de Ferrariis, O. Grizzi, M.L. Martiarena, E.A. Sánchez, Nucl. Instr. and Meth. B 232 (2005) 37.
[16] I. Aldazabal, M.S. Gravielle, J.E. Miraglia, A. Arnau, V.H. Ponce, Nucl. Instr. and Meth. B 232 (2005) 53.
[17] J.F. Ziegler, J.P. Biersack, U. Littmark, in: J.F. Ziegler (Ed.), The Stopping and Range of Ions in Matter, Vol. 1, Pergamon, New York, 1985.
[18] M.S. Gravielle, J.E. Miraglia, Phys. Rev. A 50 (1994) 2425.
[19] G. Andou, K. Nakajima, K. Kimura, Nucl. Instr. and Meth. B 160 (2000) 16.
[20] A.J. García, J.E. Miraglia, Phys. Rev. A 74 (2006) 012902.